Anionic cobalt-platinum-ethynyl (CoPt–C2H) metal-organic subnanoparticles

Aslan, Mikail; Johnston, Roy L.

DOI:
10.1140/epjb/e2018-90004-2

Document Version
Publisher's PDF, also known as Version of record

Citation for published version (Harvard):
Aslan, M & Johnston, RL 2018, 'Anionic cobalt-platinum-ethynyl (CoPt–C_2H) metal-organic subnanoparticles: a DFT modeling study', *European Physical Journal B*, vol. 91, no. 6, 120. https://doi.org/10.1140/epjb/e2018-90004-2

Eur. Phys. J. B (2018) 91: 120
https://doi.org/10.1140/epjb/e2018-90004-2

THE EUROPEAN PHYSICAL JOURNAL B

Regular Article

Anionic cobalt-platinum-ethynyl ($CoPt–C_2H$) metal-organic subnanoparticles: a DFT modeling study[⋆,⋆⋆]

Mikail Aslan[1] and Roy L. Johnston[2,a]

[1] Department of Metallurgical and Materials Engineering Gaziantep University, Gaziantep, Turkey
[2] School of Chemistry, University of Birmingham, Edgbaston, Birmingham B15 2TT, UK

Received 3 January 2018 / Received in final form 19 February 2018
Published online 18 June 2018

Abstract. Anionic CoPt-ethynyl metal-organic clusters have been investigated comprehensively. The lowest energetic of anionic Co_nPt_m(ethynyl) clusters have been generally found as 3D structure but with low symmetrical point groups. Our results indicate that the most preferred dissociation channel of the studied clusters is Co atom ejection and the favorable dissociation channel is independent of cluster size. The anionic Pt_5C_2H cluster shows the highest chemical stability according to the HOMO-LUMO Gap analysis. The C_2H generally prefers to bind on a bridge site with a few exceptions. The Co_{4-5} nanoparticles have a lengthening effect on the C≡C bond of the ethynyl molecule, which may be valuable for C≡C bond activation. In addition, the lowest and the highest vibrational frequencies are reported to guide further experimental studies.

1 Introduction

The ethynyl molecule (C_2H) is a significant reactive intermediate in hydrocarbon combustion processes [1–3]. It plays significant role in atmospheric and combustion chemistry and in catalysis [4]. It is also a widespread interstellar molecule, arising from a variety of sources [5–9]. As an interstellar molecule, C_2H is important step process in the decomposition of ethylene [10], in the transition from acetylene to ethylidyne [11], in the carbonaceous materials growth [12] and in synthesizing polyene and polyaromatic molecules [13]. In the past decades, the C_2H molecule has attracted much attention [14–17]. Ervin et al. determined the electron affinity of C_2H as 2.97 eV [18]. Zhou et al. studied C_2H and C_2D molecules by slow electron velocity-map imaging of the corresponding anions [14]. Tchatchouang et al. [19] studied stability, metastability and spectroscopic properties of some low-lying electronic states of $C_2H^-$and N_2H^-. They found that the ground state of $[C–C–H]^-$ is stable with regard to the electron detachment. Wu et al. [20] studied adsorption, hydrogenation and dehydrogenation of C_2H supported on a CoCu surface. According to their results, C_2H adsorption is greater on a single layer CoCu surface when compared to a pure Co surface.

The reactions of hydrocarbons on transition metals are among the most important industrial catalytic processes [21–26]. The interaction of transition metals with unsaturated hydrocarbons has, therefore, received significant attention [21,22,27–30]. Adsorption of a small molecule or atom may modify the electronic and magnetic properties and stability of transition metal clusters. Previous experimental and theoretical studies have been performed to investigate complexes formed between bare metal atoms and the ethynyl molecule [31–35]. The linear geometric structure of $Cr(C_2H)$ in the ground and excited states and the frequencies of $Cr(C_2H)$ around 11 100 and 13 300 cm^{-1} were reported by Brugh and coworkers [36]. By combining resonance-enhanced two-photon ionization, laser induced fluorescence, and photoionization efficiency spectroscopy experiments with density functional theory (DFT) calculations, Loock et al. determined the frequencies of different vibrational modes of $Yb(C_2H)$ [37]. $Fe(C_2H)^-$ and $Pd(C_2H)^-$ have also been studied experimentally [38,39]. Li and coworkers investigated the interaction of C_2H with small neutral and anionic gold clusters [40]. Yuan et al. investigated small anionic $Co(C_2H)$ complexes by mass spectrometry, photoelectron spectra and DFT calculations [41]. However, to date there has been no study reported on the interaction between the C_2H molecule and bimetallic clusters.

In the present work, we study anionic structures for two reasons: C_2H is generally found as anion in reaction steps and to enable comparison with existing [41] and possible future experiments. In short, We investigate the structural, energetic, electronic and magnetic properties of $[Co_nPt_m(C_2H)]^-$ $(n+m=4,5)$ nanoparticles, using DFT calculations, to understand the mechanism of formation of

⋆ Contribution to the Topical Issue "Shaping Nanocatalysts", edited by Francesca Baletto, Roy L. Johnston, Jochen Blumberger and Alex Shluger.

⋆⋆ Supplementary material in the form of one pdf file available from the Journal web page at https://doi.org/10.1140/epjb/e2018-90004-2.

[a] e-mail: r.l.johnston@bham.ac.uk

small $CoPtC_2H^-$ complexes and to address the following important questions: How does C_2H adsorption change the properties of the structure for a given cluster size? How does it change the magnetic properties of bimetallic Co–Pt clusters?

2 Computational details

The NWChem 6.0 package [42] has been used to perform geometry optimizations, and to find the total energies, the vibrational frequencies, and the energy gaps between the highest occupied and lowest unoccupied molecular orbitals (HOMO–LUMO) by DFT calculations. "CRENBL" [43] basis sets and relativistic effective core pseudopotentials (ECPs) have been chosen for Pt, where the outer most 18 valence electrons ($5s^25p^65d^96s^1$), and Co, where the outer most 17 valence electrons ($3s^23p^63d^74s^2$), are treated to reduce the number of electrons explicitly considered in the calculations. For C and H atoms, split valence 6-31G* basis sets have been employed. The reliability of the "CRENBL" basis sets and ECPs was determined by comparing atomic excitation energies with accurate all-electron calculations, i.e. if these are used, in the calculations, the maximum errors will found to be less than 0.12 eV for Pt and 0.05 eV for Co [43]. The default convergence criteria of the code have been employed: 1×10^{-6} Hartree for energies and 5×10^{-4} Hartree/a_0 for forces and BLYP exchange functional [44,45] has been chosen for the nanoalloy cluster-ethnyl complex. Firstly we calculated the lowest energetic structures of bare CoPt clusters by performing several geometry relaxation calculations starting from different morphologies. For each initial geometry, all possible homotops were subject to individual geometry optimizations. The lowest energetic structures found for bare CoPt nanoparticles were also checked with previous studies [27,28]. After finding the lowest energetic structures of bare CoPt clusters, we add the C_2H^- anion, testing all adsorption sites, including atop, bridge, and hollow sites on the CoPt structures. All geometry optimizations have been performed without symmetry constraints. Various magnetic moments were considered in the optimization, ranging from 0 to 11 μ_B.

3 Result and discussion

The optimized geometries of the low-lying isomers of anionic four and five metal atom $CoPt(C_2H)$ clusters obtained in this study are given in Figures 1 and 2 respectively. We have considered many spin multiplicities and various initial configurations (different binding sites for the CCH fragment) in these figures. Table 1 lists spin moments, binding energies per atom, HOMO-LUMO Gap (HLG), vertical detachment energies (VDEs) and highest and lowest vibrational frequencies of the studied clusters.

3.1 $[Co_mPt_n(C_2H)]^-$ $(m+n=4)$

Some of the low-lying isomers of anionic Co_mPt_n(ethynyl) clusters $(m+n=4)$ are shown in Figure 2. For these structures, VDEs range from 1.53 eV ($[Co_4(C_2H)]^-$) to 3.09 eV ($[Pt_4(C_2H)]^-$), with doping of Pt into the cluster leading to an increase in VDE.

In the lowest energy structure of the anionic Co_4(ethynyl) cluster, ethynyl is adsorbed on the bridge site with a binding energy per atom (BE) of 4.09 eV. In the study by Sebetci [46], the ground state structure of bare Co_4 was found to be a non-planar rhombus, while in other previous theoretical studies it has variously been reported to be a rhombus bent to a butterfly structure [47] and a distorted tetrahedral structure [48]. A distorted rhombus structure was found as the lowest energy isomer for $[Co_4(C_2H)]^-$ by Yuan et al. [41], which is consistent with our result (see Fig. 1). Upon ethynyl adsorption, the magnetic moment of bare Co_4 (10 μ_B) is reduced to 8 μ_B in the lowest energy isomer 1A and in the second isomer 1B (see Fig. 1), while the third isomer 1C has a spin moment of 10 μ_B and a relative energy of 0.44 eV with respect to the lowest energy structure. The energy difference between the first and second isomers is relatively small (0.09 eV).

In the study by Sebetci [49], the Co–Co and Co–Pt bond lengths of the bare Co_3Pt cluster, with a planar rhombus structure, were 2.25 Å and 2.38 Å, respectively. The adsorption of the ethynyl molecule here leads to expansion of the Co–Co bond lengths. Replacing a Co atom in the anionic Co_4-ethynyl nanoparticle by Pt also weakens the Co–Co bonds. In the second isomer of $[Co_3Pt(C_2H)]^-$ (2B), which is 0.71 eV higher in energy than isomer 2A, ethynyl adsorption occurs terminally on a Co atom: the spin state is a quartet and the average Pt–Co bond length is approximately 2.50 Å.

On replacing another Co atom by Pt, the BE and VDE of the lowest energy structure of $[Co_2Pt_2(C_2H)]^-$ become 4.70 eV and 1.87 eV, respectively. The C–C bond distance in isomer 3A is 1.30 Å, which is longer than the C≡C bond in acetylene (1.20 Å) [50] and shorter than the C=C bond in ethene (1.33 Å) [51]. Considering the spin magnetic moments, there is an abrupt decrease from 7 μ_B to 4 μ_B on going from $[Co_3Pt(C_2H)]^-$ to $[Co_2Pt_2(C_2H)]^-$. The magnetic moment of the second isomer (3B, with C_s symmetry) is 6 μ_B, while the first isomer has a magnetic moment of 1 μ_B.

Compared with the bare $CoPt_3$ (which is found as rhombus structure as we found) cluster studied by Sebetci [49], the $CoPt_3$ unit in the lowest energy structure (4A) of $[CoPt_3(C_2H)]^-$ in the present study is distorted significantly (see Fig. 1), while the $CoPt_3$ units in the second (4B) and third isomers (4C) are only perturbed slightly. This indicates that ethynyl adsorption gives rise to considerable structural change in isomer 4A. Besides obvious lengthening of the Pt–C bond length, where two carbon atoms prefer to bond to the same Pt atom, the Pt–Pt bond distance in this structure is longer than that of the corresponding bare $CoPt_3$ cluster [49]. In addition, the magnetic moment of bare $CoPt_3$ is 5 μ_B [52], while the magnetic moments of all the isomers of anionic $[CoPt_3(C_2H)]^-$ shown in Figure 1 are 3 μ_B. The total energies of the second (4B) and third isomers (4C) are 0.37 eV and 0.71 eV higher than that of isomer 4A, respectively.

In our perivious study [26], by using B3LYP exchange functional, we found the ground state structure of the Pt tetramer is a distorted tetrahedron with a triplet spin

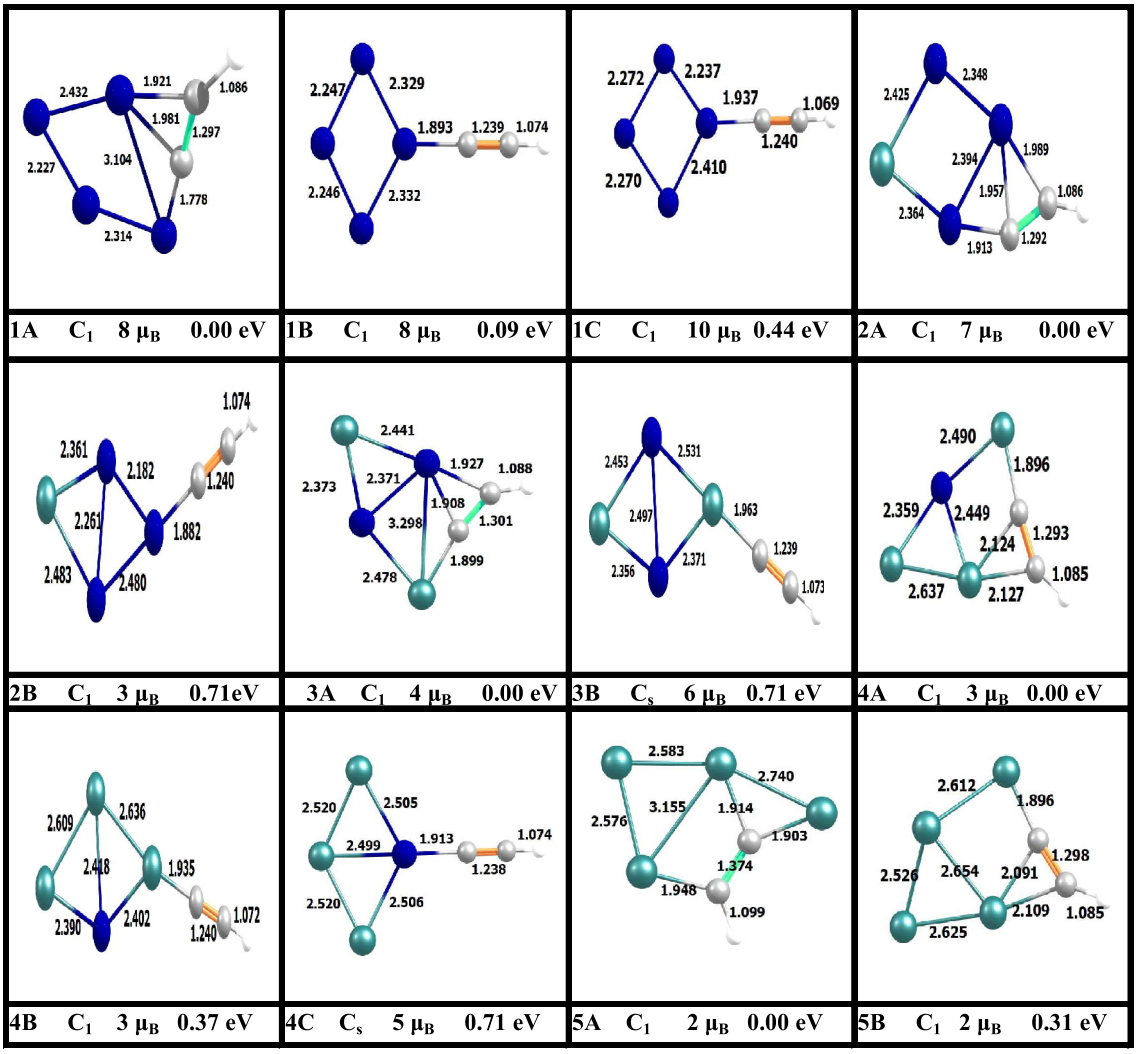

Fig. 1. The optimized structures, point group symmetries, spin moments and relative energies of some isomers of $[Co_mPt_n(C_2H)]^-(m+n=4)$. Atom colour scheme: dark blue = Co; light blue = Pt; grey = C; white = H.

state and an average Pt–Pt bond length of 2.60 Å. On the other hand, due to the adsorption of the ethynyl molecule, the Pt_4 unit in structure 5A does not preserve its tetrahedral structure in the triplet spin state. The Pt–Pt bond lengths in this particle are 2.58 Å, 2.74 Å, and 3.16 Å and the BE is 4.95 eV. On replacing the Co atom in $[CoPt_3(C_2H)]^-$ by Pt, the C–C bond distance increases. The lengthening of the C–C bond may be due to sharing of valence electrons between carbon and Pt atoms to form new Pt–C bonding interactions. In the second isomer (0.31 eV higher in energy), the tetrahedral unit of the bare Pt tetramer becomes a nonplanar rhombus, with a magnetic moment of 2 μ_B.

3.2 $[Co_mPt_n(C_2H)]^-(m+n=5)$

Some of the low-lying isomers of anionic Co_mPt_n(ethynyl) $(m+n=5)$ clusters are shown in Figure 2 While BE increases from anionic Co_5(ethynyl) to Pt_5(ethynyl), the magnitude of the change for each successive doping of Co by Pt gets smaller.

In a previous study, the ground state structure of bare Co_5 was calculated to have a planar W-shape [46], while it has also been reported to be a C_{4v} square pyramid [53], a C_{2v} rhombus pyramid [47] and a D_{3h} trigonal bi-pyramid [48,54,55]. The lowest energy structure of $[Co_5(C_2H)]^-$ obtained in the present work contains a nearly planar W-like Co_5 structure, which is consistent with the result of Yuan et al. [41], where the B3YLP xc functional was also used in their optimizations. In the ground state structure of the anionic Co_5-ethynyl cluster, carbon atoms are adsorbed at the bridge site, with a BE of 3.94 eV. The calculated VDE (1.96 eV) is close to the experimental value of 1.88 eV (see Tab. 1). For all isomers except 6D, the magnetic moment is 9 μ_B but the bare Co pentamer and the isomer 6D have high magnetic moment (11 μ_B). In the lowest energy isomers of the anionic Co_{4-5}(ethynyl) structures, the C–C bond lengths are calculated as 1.29 Å and 1.30 Å, i.e. between C≡C and C=C bond distances. Therefore, the Co_{4-5} nanoparticles have a lengthening effect on the C≡C bond of the ethynyl molecule, which may be valuable for C≡C bond activation.

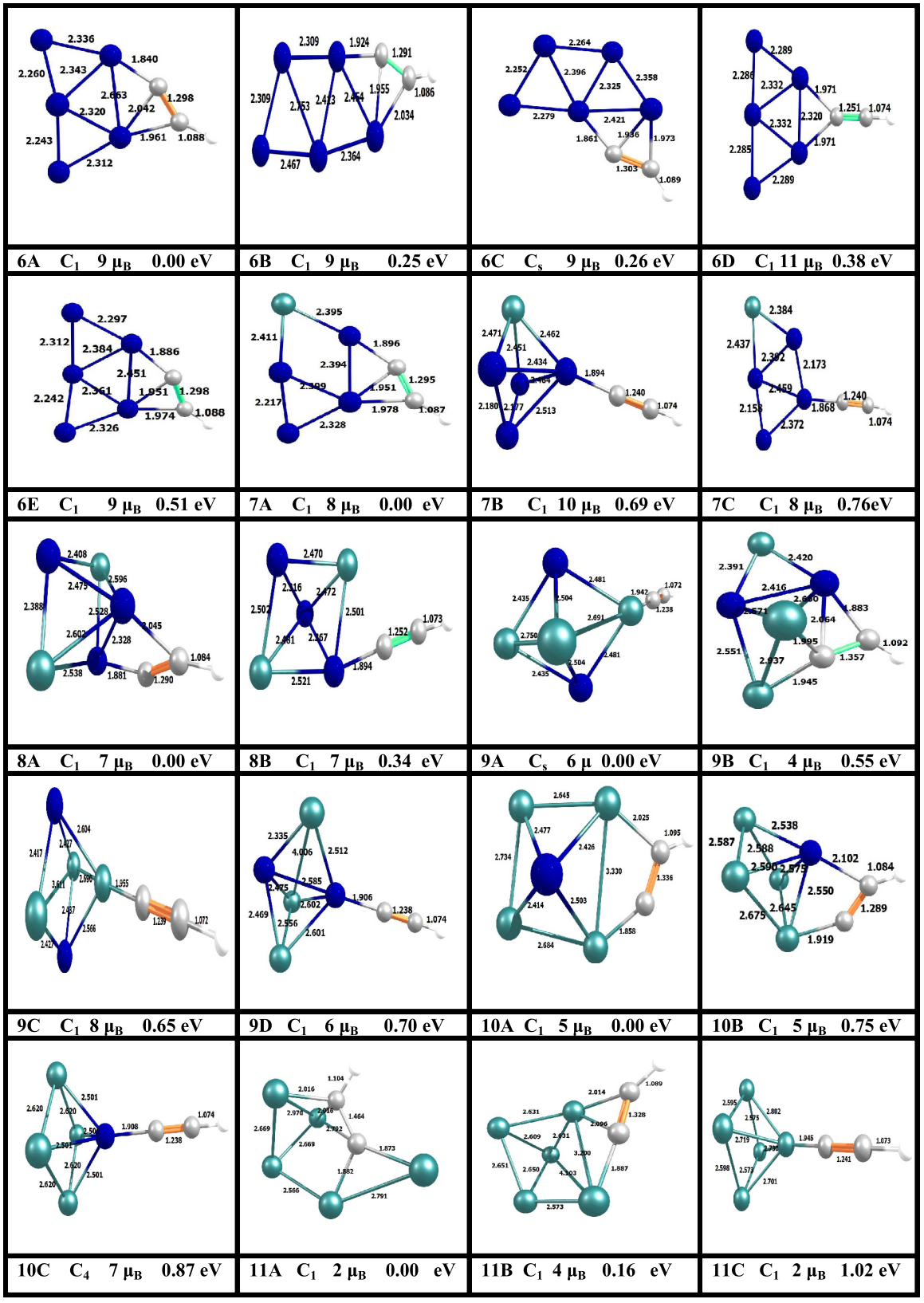

Fig. 2. The optimized structures, point group symmetries, spin moments and relative energies of some isomers of $[Co_mPt_n(C_2H)]^-$ $(m+n=5)$.

Table 1. Electronic properties of Co_nPt_m(ethynyl) clusters from DFT (BLYP) calculations.

Cluster		Spin moment (μ_B)	BE (eV)	HLG (eV)	VDE (eV)	Lowest and highest vibrational frequencies (cm^{-1})[b]
$[Co_4(C_2H)]^-$	Present work	8	4.09	0.73	1.53	171–3191
	Theoretical				1.82[a]	
	Experimental				1.63[a]	
$[Co_3Pt(C_2H)]^-$		7	4.41	0.71	1.70	58–3249
$[Co_2Pt_2(C_2H)]^-$		4	4.70	0.74	1.87	42–3175
$[CoPt_3(C_2H)]^-$		3	4.85	0.45	2.01	39–3216
$[Pt_4(C_2H)]^-$		2	4.95	0.16	3.09	28–3055
$[Co_5(C_2H)]^-$	Present work	9	3.94	0.51	1.96	65–3183
	Theoretical				2.15[a]	
	Experimental				1.88[a]	
$[Co_4Pt(C_2H)]^-$		8	4.24	0.63	2.82	35–3195
$[Co_3Pt_2(C_2H)]^-$		7	4.45	0.53	2.22	16–3224
$[Co_2Pt_3(C_2H)]^-$		6	4.64	0.76	2.63	37–3390
$[CoPt_4(C_2H)]^-$		5	4.76	0.33	2.44	25–3101
$[Pt_5(C_2H)]^-$		2	4.79	1.21	2.16	23–2975

BE: Binding energy per atom, HLG: HOMO-LUMO gap, VDE: vertical detachment energy
[a] Reference [41].
[b] Detail information is given in supplementary file.

Replacing a single Co atom in Co_5 by Pt, the lowest energy morphology does not change significantly (see Fig. 3), with two atoms moving slightly out of the plane. The Co–Pt bond lengths of the anionic Co_4Pt(ethynyl) cluster are 2.41 Å and 2.39 Å and the Co–Co distances are between 2.21 Å and 2.61 Å. The second isomer (7B) of $[Co_4PtC_2H]^-$ is constructed by atop adsorption of the C_2H molecule to one of the most highly coordinated Co atoms, with a BE of 4.76 eV. Isomer 7B, which has a distorted trigonal bipyramidal structure and a relative energy of 0.69 eV, the magnetic moment is 10 μ_B.

The 8B isomer of anionic Co_3Pt_2(ethynyl) clusters has a trigonal bipyramidal Co_3Pt_2 cluster core, where the 3 Co atoms are in the equatorial sites (with an average Co–Co bond length of 2.43 Å) and the 2 Pt atoms are on the apices of the pyramids (with an average Pt–Co bond length of 2.51 Å). In the lowest energy isomer 8A, the metal atoms form a distorted rectangular pyramid. The 8B and 8C isomers have the same magnetic moment as isomer 8A and they are 0.34 eV and 0.78 eV higher in energy, respectively, than isomer 8A.

In the ground state of the anionic Co_2Pt_3(ethynyl) structure, with a BE of 4.64 eV, the ethynyl molecule is adsorbed on the Pt side instead of Co. The spin state is a septet, which is the same as for the bare Co_2Pt_3 cluster. In all isomers except 9B (which has a relative energy of 0.55 eV), the C_2H molecule is preferentially adsorbed on an atop site. The second isomer has a magnetic moment of 4 μ_B and a C–C bond length of 1.36 Å, while isomer 9A (Cs symmetry) has a magnetic moment of 6 μ_B and a C–C bond length of 1.24 Å.

The lowest energy isomer (10A) of the anionic $CoPt_4$(ethynyl) cluster is a distorted pyramid, where 4 Pt atoms form the basal plane (with an average Pt–Pt bond length of 2.85 Å) and the Co atom is at the apex of the pyramid (with an average Co–Pt bond length of 2.46 Å). The ethynyl molecule is adsorbed on a Pt–Pt bridge site in isomer 10A. In isomer 10B (with a 5 μ_B magnetic moment), the ethynyl molecule is adsorbed on a Co–Pt bridge site. Isomer 10C has C_4 point group symmetry and the ethynyl ligand is adsorbed atop the Co atom. Isomer 10C is 0.87 eV higher in energy than 10A.

The BE of the Pt_5(ethynyl) cluster is slightly higher than that of the $CoPt_4$(ethynyl) cluster (see Tab. 1). The C–C bond length in the lowest energy isomer of $[Pt_5(C_2H)]^-$ (11A) is calculated as 1.46 Å (i.e. between a C=C double bond and a C–C single bond), where both of the C atoms are four-coordinated (forming three C-Pt bonds and one C–C bond).

3.3 Energetic analysis

Binding energy is a measure of a cluster's thermodynamic stability. Thus, to predict the relative stabilities of the Co_nPt_m(ethynyl) structures, the binding energies per atom (which is calculated as $BE = (mE[Co] + nE[Pt] + 2E[C] + E[H] + E[e^-] - E[Co_m Pt_n C_2H]^-)/(N)$, where $N = n + m + 3$) are listed in Table 1 and plotted in Figure 3. The BEs for the lowest energy structures we have studied vary from 3.94 eV to 4.95 eV. From Table 1 and Figure 3, it can be seen that the highest BE belongs to the anionic Pt_4(ethynyl) structure, while the lowest belongs to the anionic Co_5(ethynyl) species. The BEs of the clusters increase with increasing Pt doping. Provided that the size of the clusters is constant, increasing the Pt composition results in more

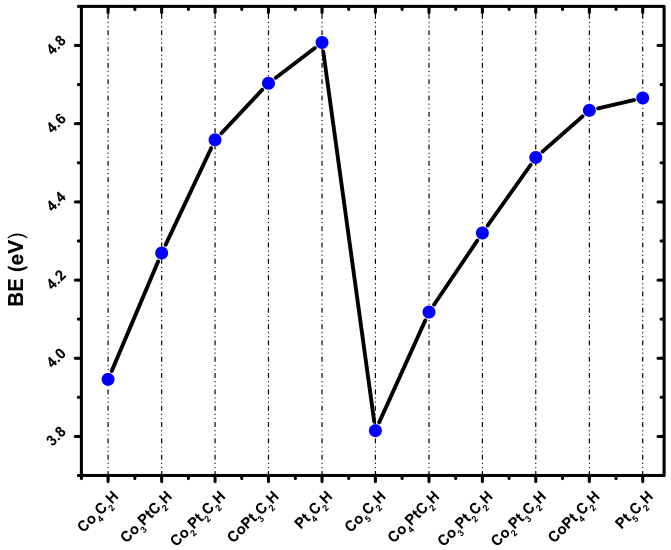

Fig. 3. The binding energy per atom (BE) of $[Co_mPt_n(C_2H)]^-$ clusters for $n + m = 4$ and 5.

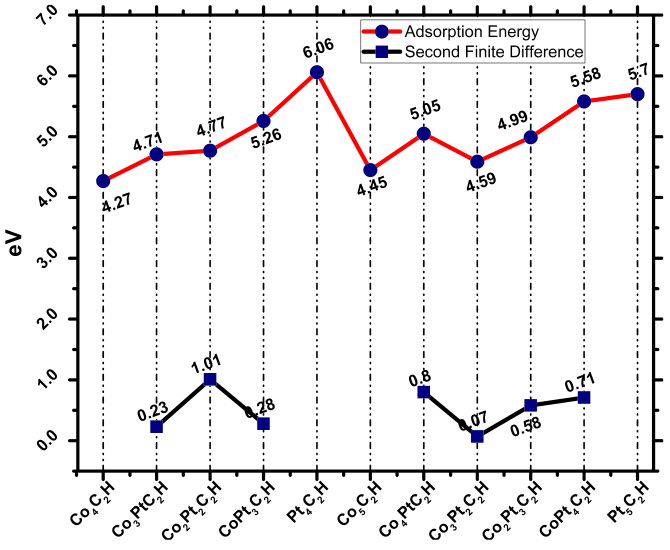

Fig. 4. The second finite difference energies ($D_{n,m}$) and C_2H^- adsorption energies (E_{ads}) of $[Co_nPt_m(C_2H)]^-$ clusters.

bonds involving Pt atoms (the Pt–Pt, Pt–Co and Pt–C bonds) and fewer Co–Co and Co–C bonds.

To further illustrate the stability of the nanoparticles and their size dependent behavior, we have calculated the second finite difference in energy, which is a quantity frequently used as a sensitive measure of the relative stability of clusters, and which is often compared directly with the relative abundances determined in mass spectroscopy experiments. Moreover, the more stable clusters are more abundant ("magic number" sizes). It was found that metal nanoparticles with certain numbers of atoms are more abundant than others. These "magic numbers" can be explained by various models, such as the jellium model [56,57]. The second finite difference energies ($D_{n,m}$) are calculated as:

$$D_{n,m} = E_{n+1,m-1} + E_{n-1,m+1} - 2E_{n,m}, \quad (1)$$

where $E_{n,m}$ is the total energy of the $[Co_nPt_m(C_2H)]^-$ cluster. The second finite differences in energies of the studied clusters are plotted in Figure 5. The noticeable peak in $D_{n,m}$ for Co_nPt_m ($m = n = 2$) indicates that the $[Co_2Pt_2(C_2H)]^-$ cluster is more stable than the neighboring clusters. The anionic Co_3Pt_2(ethynyl) structure can be considered the least stable structure, as it corresponds to a dip in the $D_{n,m}$ plot for $n + m = 5$.

In order to assess the bonding strength between neutral Co_nPt_m ($n + m = 4$ and 5) clusters and the $(C_2H)^-$ anion, we calculated the adsorption energies (E_{ads}, which are plotted in Fig. 4) as:

$$E_{ads} = E[Co_nPt_m] + E[(C_2H)^-] - E[Co_nPt_m(C_2H)^-], \quad (2)$$

where $E[*]$ is the total energy of a given species in the equation. The adsorption energies reveal an increase with increasing Pt/Co ratio. The trend has no exception for the structures with tetrametallic units. A peak in the adsorption energies is seen in Figure 4 for $[Pt_4(C_2H)]^-$, while the adsorption energy of $[Co_5(C_2H)]^-$ corresponds to a dip in the plot. These two clusters have ethynyl adsorption energies of 6.09 eV and 4.45 eV, respectively. Furthermore, for anionic Co_{4-5}(ethynyl) clusters, the increase in the size of the cluster leads to a slight increase in the adsorption energy.

Another sensitive quantity that reflects relative stability is the dissociation energy. For the anionic Co_nPt_m(ethynyl) species, the dissociation channels

$$[Co_nPt_m(C_2H)]^- \rightarrow [Co_{n-x}Pt_{m-y}(C_2H)]^- + [Co_xPt_y]$$

are investigated and the corresponding dissociation energies (E_{dis}) are computed as:

$$E_{dis} = -E[Co_nPt_m(C_2H)^-] + E[Co_xPt_y] + E[Co_{n-x}Pt_{m-y}(C_2H)^-]. \quad (3)$$

The selected dissociation channels and the corresponding dissociation energies are listed in Table 2. The most favorable dissociation channels correspond to the minimum dissociation energies. From our DFT calculations, when $n + m$ is odd, clusters usually dissociate via loss of a Co or Pt monomer, yielding an even-atom product cluster. This is consistent with experimental results on cationic and anionic metal clusters [58–60], where small odd-numbered clusters were found to evaporate a neutral monomer. On the other hand, when $n + m$ is even, the clusters sometimes favor loss of a dimer (preferably Co_2 or CoPt), resulting in another even-atom cluster.

For pure Pt(ethynly) and Co(ethynly) clusters, as shown in Table 2, the dissociation of Pt_2 and Co_2 dimers is favored over monomer dissociation for Pt_4 and Co_4, by 0.24 eV and 0.20 eV, respectively. For Co_5, monomer loss is favored over dimer dissociation by 0.24 eV, while for Pt_5

Table 2. Dissociation energies for selected anionic Co_nPt_m(ethynyl) clusters.

Clusters	Dissociation channel	E_{dis} (eV)
$[Co_4(C_2H)]^-$	$[Co_2(C_2H)]^- + Co_2$	2.68
$[Co_4(C_2H)]^-$	$[Co_3(C_2H)]^- + Co$	2.88
$[Co_3Pt(C_2H)]^-$	$[Co_3(C_2H)]^- + Pt$	5.14
$[Co_3Pt(C_2H)]^-$	$[Co_2Pt(C_2H)]^- + Co$	2.61
$[Co_2Pt_2(C_2H)]^-$	$[CoPt(C_2H)]^- + CoPt$	3.53
$[Co_2Pt_2(C_2H)]^-$	$[Pt_2(C_2H)]^- + Co_2$	3.99
$[Co1Pt_3(C_2H)]^-$	$[Co_2Pt(C_2H)]^- + CoPt$	3.03
$[Pt_4(C_2H)]^-$	$[Pt_3(C_2H)]^- + Pt$	4.29
$[Pt_4(C_2H)]^-$	$[Pt_2(C_2H)]^- + Pt_2$	4.05
$[Co_5(C_2H)]^-$	$[Co_4(C_2H)]^- + Co$	2.90
$[Co_5(C_2H)]^-$	$[Co_3(C_2H)]^- + Co_2$	3.14
$[Co_5(C_2H)]^-$	$[Co_2(C_2H)]^- + Co_3$	3.24
$[Co_4Pt(C_2H)]^-$	$[Co_3Pt(C_2H)]^-$+ Co	3.06
$[Co_4Pt(C_2H)]^-$	$[Co_2Pt(C_2H)]^-$+ Co_2	3.03
$[Co_4Pt(C_2H)]^-$	$[CoPt(C_2H)]^- + Co_3$	3.56
$[Co_3Pt_2(C_2H)]^-$	$[Co_2Pt_2(C_2H)]^- + Co$	2.65
$[Co_3Pt_2(C_2H)]^-$	$[CoPt_2(C_2H)]^-$+ Co_2	3.56
$[Co_3Pt_2(C_2H)]^-$	$[Co_2Pt(C_2H)]^-$+CoPt	3.31
$[Co_3Pt_2(C_2H)]^-$	$[Co_3(C_2H)]^- + Pt_2$	5.50
$[Co_2Pt_3(C_2H)]^-$	$[Co_2(C_2H)]^- + Pt_3$	5.81
$[Co_2Pt_3(C_2H)]^-$	$[CoPt_2(C_2H)]^-$+Co	3.18
$[Co_2Pt_3(C_2H)]^-$	$[CoPt_2(C_2H)]^-$ +CoPt	3.77
$[Co_2Pt_3(C_2H)]^-$	$[CoPt_3(C_2H)]^-$ +Co	3.4
$[Pt_5(C_2H)]^-$	$[Pt_4(C_2H)]^-$ +Pt	3.67
$[Pt_5(C_2H)]^-$	$[Pt_3(C_2H)]^- + Pt_2$	3.65
$[Pt_5(C_2H)]^-$	$[Pt_2(C_2H)]^- + Pt_3$	4.04

they are approximately degenerate. For the pure clusters, as CCH^- is an even electron species, an odd number of Co atoms leads to a cluster with an odd number of electrons. Loss of a single (odd electron) Co atom leads to an even-electron cluster which should be locally stable. If the number of Co atoms is even, then the cluster has an even number of electrons so loss of a single Co atom would create an odd-electron product, which is unfavorable. As a Pt atom has an even number of electrons, there is no even-electron driving force favoring loss of one over two Pt atoms.

For mixed CoPt clusters, Table 2 shows that the dissociation energy of a single Pt atom is higher than that of Co. This is consistent with the trend in BEs mentioned above and is due to the greater strength of bonds involving Pt atoms. The most favorable reactions are:

$$[Co_3Pt(C_2H)]^- \rightarrow [Co_2Pt(C_2H)]^- + Co$$
$$[Co_3Pt_2(C_2H)]^- \rightarrow [Co_2Pt_2(C_2H)]^- + Co$$

since their dissociation energies have the lowest values in Table 2. On the other hand, the least favorable reactions are:

$$[Co_2Pt_3(C_2H)]^- \rightarrow [Co_2(C_2H)]^- + Pt_3$$
$$[Co_3Pt_2(C_2H)]^- \rightarrow [Co_3(C_2H)]^- + Pt_2$$

since they have the highest dissociation energies.

The HOMO energy is related to the ability of the cluster to donate an electron, whereas the LUMO energy is an indicator of electron acceptance. The energy gap between HOMO and LUMO reveals the ability of electrons to migrate from HOMO to LUMO. A large HLG has been considered as significant requirement for chemical stability [26].

The calculated HLGs and lowest and highest vibrational frequencies are presented in Table 1. We have also plotted the HLGs and VDEs of the $[Co_nPt_m(C_2H)]^-$ species in Figure 5. It is evident that the adsorption of the C_2H molecule tends to decrease the energy gap for $[Pt_{4-5}(C_2H)]^-$, indicating that the clusters become more conductive, while for $[Co_{4-5}(C_2H)]^-$, it tends to increase the energy gap, indicating that the clusters become more stable. According to Table 1, $[Pt_5(C_2H)]^-$ possesses high chemical stability due to its large HLG (1.21 eV) when compared to the other species.

VDE is expressed as the minimum energy needed to eject an electron from the negative ion in its ground state. The VDE results we have calculated for $[Co_{4-5}(C_2H)]^-$, as well as other theoretical results and the corresponding experimental values [41], are listed in Table 1. The calculated VDE values in the present study are in agreement with the previous results [41]. The peak in VDE (see Fig. 5) is 3.09 eV for $[Pt_4(C_2H)]^-$, while a dip (1.96 eV) is seen at $[Co_5(C_2H)]^-$. Though the VDE increases with increasing number of Pt atoms in clusters with $n+m=4$, it oscillates for $n+m=5$.

The lowest and highest vibrational frequencies of the lowest energy isomers of all the species studied in the present work are given in Table 1. For future experimental vibrational spectral analysis, the detailed information

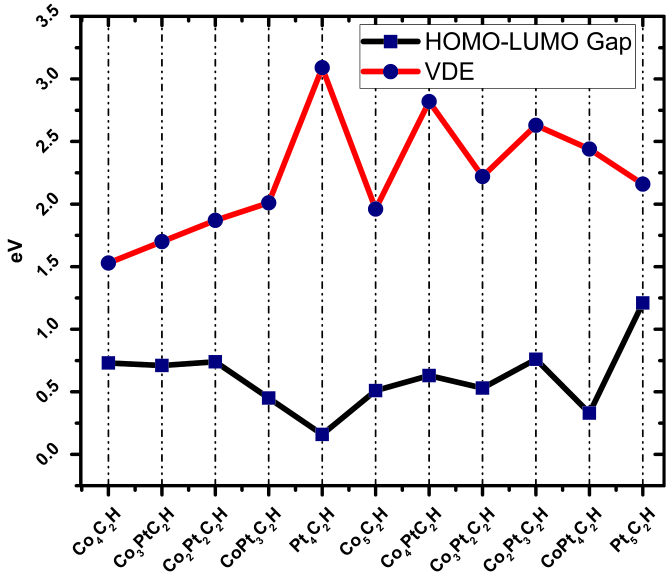

Fig. 5. The HOMO-LUMO gaps and VDEs of $[Co_nPt_m(C_2H)]^-$ clusters ($n + m = 4$ and 5).

including all vibrational frequencies and projected infra red intensities are given in supplementary file.

4 Conclusions

DFT results indicate that the ground state structures of small bimetallic anionic Co_nPt_m(ethynyl) clusters are generally three-dimensional structures with low symmetry. Alloying with Pt atoms leads to an increase in the binding energy of the clusters. The C_2H^- anion generally prefers to bind on a bridge site with a few exceptions. The species $[Co_2Pt_2(C_2H)]^-$, $[Co_4Pt(C_2H)]^-$ and $[CoPt_4(C_2H)]^-$ are found to be more stable than their neighboring sizes, since they have relatively high second finite difference energies. The highest HOMO-LUMO gap is found for $[Pt_5(C_2H)]^-$, which indicates high chemical stability. The preferred dissociation channel of anionic Co_nPt_m(ethynyl) clusters is Co atom ejection, with the dissociation energy being relatively independent of cluster size. In addition, ethynyl adsorption leads to a weak quenching of the magnetic moments on the Co_nPt_m clusters.

This research is supported by the Scientific and Technological Research Council of Turkey, under the program 2214-A. The calculations reported here have been performed partly on The University of Birmingham BlueBEAR HPC facility (see http://www.bear.bham.ac.uk/bluebear for details).

Author contribution statement

MA designed the research project and carried out the calculations. MA and RLJ both analyzed the results and wrote the paper.

References

1. J.H. Kiefer, W.A. Von Drasek, Int. J. Chem. Kinetics **22**, 747 (1990)
2. W. Boullart, K. Devriendt, R. Borms, J. Peeters, J. Phys. Chem. **100**, 998 (1996)
3. J. Kiefer, S. Sidhu, R. Kern, K. Xie, H. Chen, L. Harding, Combust. Sci. Technol. **82**, 101 (1992)
4. W. Feng, J.F. Hershberger, J. Phys. Chem. A **117**, 3585 (2013)
5. A. Dutrey, S. Guilloteau, M. Guelin, Astron. Astrophys. **317**, L55 (1997)
6. A. Wootten, E. Bozyan, D. Garrett, R. Loren, R. Snell, Astrophys. J. **239**, (1980)
7. A. Olofsson, C.M. Persson, N. Koning, P. Bergman, P. Bernath, J.H. Black, U. Frisk, W. Geppert, T. Hasegawa, A. Hjalmarson, arXiv:0910.1825 (2009)
8. K. Tucker, M. Kutner, P. Thaddeus, Astrophys. J. **193**, L115 (1974)
9. R. Lucas, H. Liszt, Astron. Astrophys. **358**, 1069 (2000)
10. D. Basaran, H.A. Aleksandrov, Z.-X. Chen, Z.-J. Zhao, N. Rösch, J. Mol. Catal. A: Chem. **344**, 37 (2011)
11. X. Lu, L. Liu, Y. Li, W. Guo, L. Zhao, H. Shan, Phys. Chem. Chem. Phys. **14**, 5642 (2012)
12. W. Zhang, P. Wu, Z. Li, J. Yang, J. Phys. Chem. C **115**, 17782 (2011)
13. T. Kovács, M.A. Blitz, P.W. Seakins, J Phys. Chem. A **114**, 4735 (2010)
14. J. Zhou, E. Garand, D.M. Neumark, J. Chem. Phys. **127**, 114313 (2007)
15. R.A. Shepherd, W.R.M. Graham, J. Chem. Phys. **86**, 2600 (1987)
16. Y.C. Hsu, Y.J. Shiu, C.M. Lin, J. Chem. Phys. **103**, 5919 (1995)
17. Y.-J. Wu, B.-M. Cheng, Chem. Phys. Lett. **461**, 53 (2008)
18. K.M.L. Ervin, W.C. Lineberger, Chem. Phys. Lett. **95**, 1167 (1991)
19. M. Tchatchouang, M. Nsangou, O. Motapon, Comput. Theor. Chem. **1117**, 241 (2017)
20. D. Wu, J. Yuan, B. Yang, H. Chen, Surf. Sci. **671**, 36 (2018)
21. Q. Lin, K. Aguirre, S.M. Saunders, T.A. Hackett, Y. Liu, V. Taufour, D. Paudyal, S. Budko, P.C. Canfield, G.J. Miller, Chemistry **23**, 10516 (2017)
22. N. Li, X. Chen, W.-J. Ong, D. R. MacFarlane, X. Zhao, A. K. Cheetham, C. Sun, ACS Nano **11**, 10825 (2017)
23. Y. Sun, H. Tang, K. Chen, L. Hu, J. Yao, S. Shaik, H. Chen, J. Am. Chem. Soc. **138**, 3715 (2016)
24. L. Souillart, N. Cramer, Chem. Rev. **115**, 9410 (2015)
25. Y.N. Regmi, G.R. Waetzig, K.D. Duffee, S.M. Schmuecker, J.M. Thode, B.M. Leonard, J. Mater. Chem. A **3**, 10085 (2015)
26. M. Aslan, Z. Öztürk, A. Sebetci, J. Clust. Sci. **25**, 1187 (2014)

27. A. Zaleska-Medynska, M. Marchelek, M. Diak, E. Grabowska, Adv. Colloid Interface Sci. **229**, 80 (2016)
28. G.-N. Yun, A. Takagaki, R. Kikuchi, S.T. Oyama, Catal. Sci. Technol. **7**, 281 (2017)
29. A. Galadima, O. Muraza, J. Ind. Eng. Chem. **29**, 12 (2015)
30. Y. Park, Y. Kim, S. Chang, Chem. Rev. **117**, 9247 (2017)
31. M. Anderson, L. Ziurys, Astrophys. J. **439**, L25 (1995)
32. B.P. Nuccio, A.J. Apponi, L.M. Ziurys, Chem. Phys. Lett. **247**, 283 (1995)
33. M. Anderson, L. Ziurys, Astrophys. J. **444**, L57 (1995)
34. A.M.R.P. Bopegedera, C.R. Brazier, P.F. Bernath, J. Mol. Spectrosc. **129**, 268 (1988)
35. M.A. Brewster, A.J. Apponi, J. Xin, L.M. Ziurys, Chem. Phys. Lett. **310**, 411 (1999)
36. D.J. Brugh, R.S. DaBell, M.D. Morse, J. Chem. Phys. **121**, 12379 (2004)
37. H.-P. Loock, A. Bérces, B. Simard, C. Linton, J. Chem. Phys. **107**, 2720 (1997)
38. J. Fan, L.-S. Wang, J. Phys. Chem. **98**, 11814 (1994)
39. V.D. Moravec, S.A. Klopcic, C.C. Jarrold, J. Chem. Phys. **110**, 5079 (1999)
40. D.-Z. Li, M.-Z. Song, Q.-H. Xu, S.-G. Zhang, J. Clust. Sci. **23**, 481 (2012)
41. J. Yuan, H.-G. Xu, Z.-G. Zhang, Y. Feng, W. Zheng, J. Phys. Chem. A **115**, 182 (2010)
42. M. Valiev, E.J. Bylaska, N. Govind, K. Kowalski, T.P. Straatsma, H. J. Van Dam, D. Wang, J. Nieplocha, E. Apra, T.L. Windus, Comput. Phys. Commun. **181**, 1477 (2010)
43. M.M. Hurley, L.F. Pacios, P.A. Christiansen, R.B. Ross, W.C. Ermler, J. Chem. Phys. **84**, 6840 (1986)
44. A.D. Becke, Phys. Rev. A **38**, 3098 (1988)
45. C. Lee, W. Yang, R.G. Parr, Phys. Rev. B **37**, 785 (1988)
46. A. Sebetci, Chem. Phys. **354**, 196 (2008)
47. Q.-M. Ma, Z. Xie, J. Wang, Y. Liu, Y.-C. Li, Phys. Lett. A **358**, 289 (2006)
48. S. Datta, M. Kabir, S. Ganguly, B. Sanyal, T. Saha-Dasgupta, A. Mookerjee, Phys. Rev. B **76**, 014429 (2007)
49. A. Sebetci, J. Magn. Magn. Mater. **324**, 588 (2012)
50. J.A. Dean, *Properties of atoms, radicals, and bonds*, 4th edn. (1999)
51. H. Zhou, H. Tamura, S. Takami, M. Kubo, R. Belosloudov, N. Zhanpeisov, A. Miyamoto, Appl. Surf. Sci. **158**, 38 (2000)
52. S. Akbayrak, M. Kaya, M. Volkan, S. Özkar, Appl. Catal. B: Environ. **147**, 387 (2014)
53. H.-J. Fan, C.-W. Liu, M.-S. Liao, Chem. Phys. Lett. **273**, 353 (1997)
54. J.L. Rodríguez-López, F. Aguilera-Granja, K. Michaelian, A. Vega, Phys. Rev. B **67**, 174413 (2003)
55. M. Pereiro, S. Man'kovsky, D. Baldomir, M. Iglesias, P. Mlynarski, M. Valladares, D. Suarez, M. Castro, J.E. Arias, Comput. Mater. Sci. **22**, 118 (2001)
56. O. Echt, K. Sattler, E. Recknagel, Phys. Rev. Lett. **47**, 1121 (1981)
57. W.-D. Knight, K. Clemenger, W.A. de Heer, W.A. Saunders, M. Chou, M.L. Cohen, Phys. Rev. lett. **52**, 2141 (1984)
58. K. Hansen, J.U. Andersen, J.S. Forster, P. Hvelplund, Phys. Rev. A **63**, 023201 (2001)
59. V.A. Spasov, T.H. Lee, K.M. Ervin, J. Chem. Phys. **112**, 1713 (2000)
60. M. Vogel, K. Hansen, A. Herlert, L. Schweikhard, Appl. Phys. B: Lasers Opt. **73**, 411 (2001)